

# A compact energy harvesting multiband rectenna based on metamaterial complementary split ring resonator antenna and modified hybrid junction ring rectifier

Ali Benayad  | Mohamed Tellache

Laboratory of Instrumentation (LINS),  
Faculty of Electronics and Computer  
Science, University of Science and  
Technology Houari Boumediene, Algiers,  
Algeria

## Correspondence

Ali Benayad, Laboratory of  
Instrumentation (LINS), Faculty of  
Electronics and Computer Science,  
University of Science and Technology  
Houari Boumediene, BP 32, El-Alia,  
16025, Bab-Ezzouar, Algiers, Algeria.  
Email: abenayad@usthb

## Abstract

This article presents an improved wireless energy harvesting multiband rectifying antenna. The proposed design is based on an original optimized bidirectional complimentary split ring resonator (CSRR) metamaterial multiband antenna and a modified hybrid junction ring rectifier with four rectifying branches. It harvests the ambient radiofrequency radiations at GSM, 1.8 GHz; UMTS, 2.1 GHz; WiFi, 2.45 GHz; and 4G-2.6 GHz GSM bands. The created prototypes are printed on a 1.57-mm-thickness FR4 substrate and achieve the needed dimensional optimization in both antenna and rectifier. The CSRR antenna accomplished a maximum harvesting realized gain of 2.41, 2.26, 1.58, and 2.69 dB on the aforementioned frequency bands, respectively, 63.75% of antenna size reduction, and 23.62% rectifier size reduction regarding the conventional designs. The hybrid ring junction is used to independently match the subrectifiers at each frequency band. The realized rectenna has been accurately tested in both controlled and outdoor environments, achieving a 67.6% peak efficiency at 1.8 GHz frequency band for an input power level of 10 dBm. It powered up a digital batteryless watch in the outdoor experiment.

## KEY WORDS

complimentary Split ring resonator, modified hybrid junction ring, multiband antenna, RF energy harvesting, RF rectifier

## 1 | INTRODUCTION

The last decade has witnessed an immense technological revolution, in which electronic devices became exponentially miniaturized, more efficient, and less energy consuming. Unfortunately, the energy supply and storage systems could not follow the chase, mainly, because of their dimensional and weight bulkiness. In addition, the supplying systems and batteries are dependent on their regular rechargeability and narrow lifetime compared with that of the device. Among the variety of the globally proposed solutions (such as solar, piezoelectric, and thermal),

harvesting the ambient electromagnetic power emerges as an attractive solution to expand the power supplier's lifetime or even replace it. A rectifying antenna (Rectenna) is a system that harvests and converts the ambient RF energy into useful DC power via an antenna followed and matched to a rectifying circuit and a resistive load. In the literature, researchers focused their studies on harvesting a single-frequency ambient energy, which is mostly 2.45 GHz,<sup>1–3</sup> since it is the less affected by the air attenuations.<sup>4</sup> However, the emitted energy by the 2.45 GHz sources is very low compared with some other existing ambient frequencies. Numerous works have tried to enhance the harvesting

efficiency by using dual<sup>5-9</sup> or broad band antennas,<sup>10,11</sup> which improves the results at the expense of the antenna's size and put in question the embeddability of the whole system. Furthermore, the broadband antennas come with either a low transmission gain or a feeble reflection coefficient, which reduces its efficiency.<sup>6</sup> In order to solve this dilemma, we had to look for technologies that can reduce the size of the antenna, achieve the multiband resonance at the frequency bands of interests, and efficiently convert the harvested RF energy to a useful DC power.

The purpose of this article is to propose an optimized energy harvesting rectenna constituted of a multiband metamaterial unit cell antenna that resonates at the following frequency bands: GSM 1.8 GHz; UMTS 2.1 GHz; Wi-Fi and bluetooth 2.45 GHz; and 4G 2.6 GHz GSM bands, and an efficient multiband modified hybrid ring junction rectifier, thus improving the harvesting efficiency by increasing the energy sources number. Metamaterials were firstly introduced in 1968 by Veselago.<sup>12</sup> They are artificially engineered homogenous materials that exhibit some interesting properties and dielectric characteristics that cannot be found in natural materials, particularly, negative refractive index for which the permittivity and permeability have simultaneously negative values (DGN). Furthermore, they lead to potential applications, many of which were considered impossible in the past such as invisibility cloaking<sup>13</sup> and miniaturizing microwave devices.<sup>14</sup>

Literature reviews suggest that the major requirements to choose an energy-harvesting antenna are as follows: bandwidth at the resonance frequency and the harvesting efficiency. In this article, we extend and verify the approach proposed in Reference 15, furthermore, we suggest a new designed metamaterial rectenna by using an optimized bidirectional four-banded CSRR unit cell antenna followed by a hybrid junction ring rectifier that matches the antenna with the voltage doublers and filters the signals each to its specific Schottky voltage doubler output branch. The optimized rectenna design allows the system to harvest the fundamental ambient frequency bands and makes it more suitable for embedded applications. In the present work, we mainly deal with both antenna's and rectifier's size reductions and also the harvesting efficiency enhancement when compared with conventional rectennas that work on the same frequency bands. The remainder of the article is organized as follows. Section 2 highlights the theoretical approach and provides a description of the design procedure, outlining the simulation results of the antenna. The proposed modified hybrid ring junction matching and rectifying circuits is discussed in Section 3. Section 4 provides experimental results. Finally, Section 5 concludes with a summary and some open enhancements.

## 2 | THE OPTIMIZED CSRR ANTENNA DESIGN

In Reference 15, the authors have studied the performances of the individual SRR unit cell based on the spiral inductors modeling methods in monolithic microwave integrated circuit, and they proposed the corrected mathematical model predicting the behavior of the two ring SRR-based metamaterials that exhibit left-handed properties over multiple frequency bands. By investigating the results reported in References 15-19, we noticed that the applied method can be an effective way to harvest the ambient energy of multiple frequency bands by creating an optimized and efficient complimentary unit of the SRR cell antenna that can resonate at the four needed frequencies. According to the Babinet principle, the complementary split ring resonator structure is obtained by replacing the copper parts of the original structure with air and vice versa. Hence, due to the duality theorem, these two structures have approximately the same resonance frequency. The main difference between SRR and CSRR is that SRR has negative permeability characteristics, while CSRR has negative permittivity characteristics. Moreover, the resonance phenomenon in quasistatic resonators such as CSRR and SRR is a result of the interaction of the distributed capacitance and inductance of the structure, which considerably reduces their size comparing to the conventional resonators of which dimensions are comparable to the wavelength, where the resonance phenomenon is based on phase propagation.<sup>19,20</sup> In both cases, the resonance frequency can be approximately formulated as<sup>15,19</sup>:

$$f_n = \frac{1}{2\pi\sqrt{L_D C_n}} \quad (1)$$

where  $L_D$  and  $C_n$  are the distributed inductance and capacitance in the structure, respectively.

Reminding that the study in Reference 15 has been elaborated on two rings of individual SRR waveguide that generates three resonance frequencies based on the presented model. The simulation results of the aforementioned in Reference 15 indicate that studied individual SRR cell has manifested an almost full reflective behavior at the three resonance frequencies, and according to References 19 and 21, the complementary structure switches the reflective behavior of the SRR into pass-band.<sup>21-23</sup> In order to verify the validity of the proposed method, several experiments and simulations have been carried out by using CST microwave studio to achieve the final result.

Based on Reference 15 and referring to the square spiral inductors lumped circuit models, the SRR equivalent inductors and capacitances are approximately estimated by the four side parts of the structure, as shown in Figure 1,

namely L1, L2, L3, and L4, respectively, for the inductors and C1, C2, C3, and C4, respectively, for the capacitances, which can be determined as follows<sup>15,23</sup>:

$$L_D = \frac{K\mu_0 n^2 L}{2\pi} \left[ \ln\left(\frac{2}{\rho}\right) + 0.5 + 0.178\rho + 0.0146\rho^2 + \frac{0.5(n-1)S^2}{(\rho n)^2} + 0.178\frac{(n-1)S}{n} - \frac{1}{n}\ln\left(\frac{W+t}{W}\right) \right] \quad (2)$$

$$\rho = \frac{nW + (n-1)S}{L} \quad (3)$$

$$k = \frac{(2L-2S)-D}{(2L-2S)} \quad (4)$$

where  $n$  is the number of rings,  $W$  is the ring width,  $L$  is the length of outer ringsides,  $S$  is the space between rings,  $D$  is the gap width, and  $t$  is the ring's thickness.

The total capacitance in each of the SRR four sides consists of two parts. One part is the coupling capacitance between the rings, which will be divided into four equal counterparts named  $C_0$  for the four sides of the SRR, and the other one  $C_{Di}$  is produced by the accumulated electric charges at the gaps splits,<sup>17,18</sup> hence

$$C_0(pF) = \frac{1}{4} * [0.06 + 3.5*10^{-5}(R_{out} + R_{in})] \quad (5)$$

$$C_{Di} = \epsilon_r \epsilon_0 \frac{W*t}{Di} \quad (6)$$

where  $R_{out}$  and  $R_{in}$  represent the radius of the outer circumcircle and the inner circumcircle of SRR, respectively. Therefore, the final expression of the capacitance for each side of the antenna can be expressed as follows:

$$C_1 = C_0 + C_{D1} \quad (7)$$

$$C_2 = C_0 + C_{D2} \quad (8)$$

$$C_3 = C_0 + C_{D3} \quad (9)$$

$$C_4 = C_0 + C_{D4} \quad (10)$$

Since the frequency bands of interest are in very close range, the structure could not have achieved the needed results if the same gap size was maintained, accordingly, we had to consider a different gap size ( $D_i$ ) for each side of the antenna. Therefore, the geometry of the SRR has been adjusted to resonate at the needed frequency bands

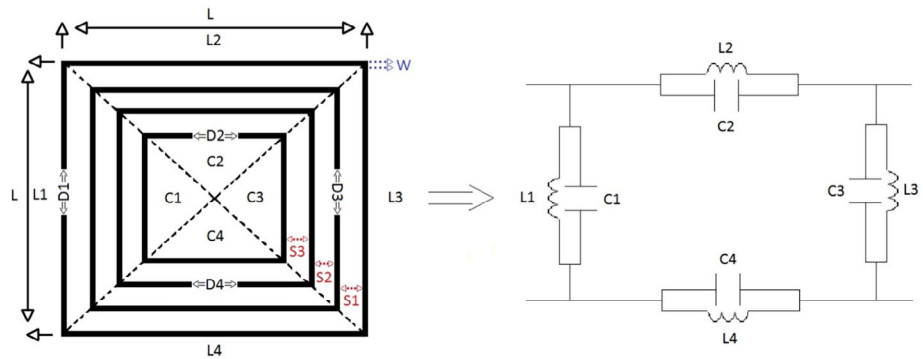


**FIGURE 1** The geometry configuration and the lumped element distribution in equivalent circuit model of the proposed individual square SRR

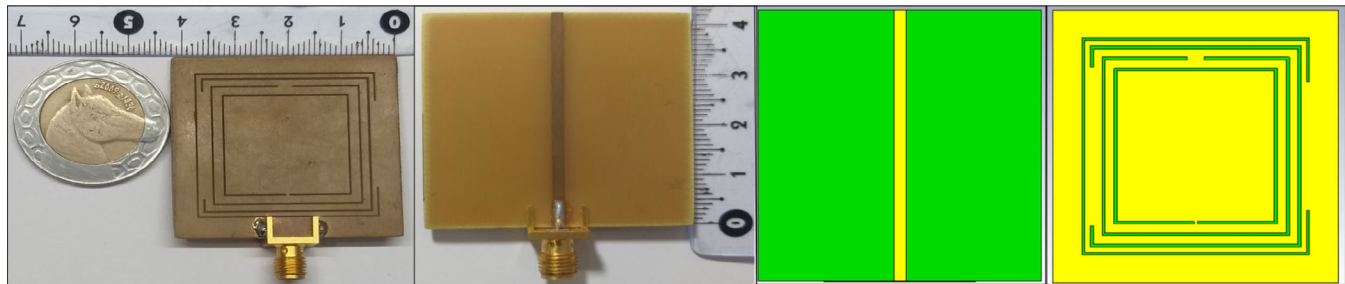


**FIGURE 2** The simulated and realized configurations of the complimentary structure of the calculated SSR unit cell as a multiband antenna

**TABLE 1** Geometrical parameters of the CSRR/SRR/multiband unit cell antenna (unit: mm)

Parameter	<b>L</b>	<b>W</b>	<b>T</b>	<b>S<sub>1</sub></b>	<b>S<sub>2</sub></b>	<b>S<sub>3</sub></b>	<b>D<sub>1</sub></b>	<b>D<sub>2</sub></b>	<b>D<sub>3</sub></b>	<b>D<sub>4</sub></b>
Value	42.8	0.4	0.1	0.8	1.3	1.4	25	2.5	20.2	0.5

through modifying the gap resulting capacitance in each ring by increasing or decreasing its size from the first standard value.

The initial stage of the simulations has been devoted to verify the approach and reduce the dimensions range in order to achieve the needed frequencies. After adjusting the first geometry by varying the four gap widths (each corresponding to one frequency band of interest), the structure has been tuned and the space between each ring ( $\text{Si}$ ) of the SRR was adjusted, to finally complete and approve the design.

After tuning the final SRR geometry to resonate at the frequency bands of interest in which the antenna has a reflective behavior, simulations have been carried out with

its complimentary structure to reverse the reflective behavior into passbands at the same resonance frequencies as achieved in References 20-22. Figure 2 illustrates the simulated and realized complimentary design of the final calculated SRR at the needed frequency bands of interest. The simulated antenna has been fabricated by using FR4-PCB that has a dielectric constant  $\epsilon_r = 4.3$  and a loss factor  $\tan \delta = 0.02$  where the copper thickness is  $t = 0.035$  mm.

The final geometrical parameters of the proposed multiband antenna are listed in Table 1. The antenna has been designed to resonate at the following frequency bands: 1.8, 2.1, 2.45, and 2.6 GHz.

After simulating and tuning the geometry to resonate at the frequency bands of interest and then, fabricating the antenna, the simulated and measured reflection coefficient behaviors have been compared to the simulated reflection coefficient of the antenna without the SRR engraving. The results are shown in Figure 3. The measured reflection coefficient variations were taken by using a Rohde & Schwarz ZVH4 cable and an antenna analyzer.

The variations depict a good agreement between the obtained results and the expected goals where the antenna resonates efficiently at the four wanted frequencies. In addition, one notes that the unit cell antenna shows a bidirectional behavior as illustrated in Figure 4 at all the frequency bands of interest, which supports its suitability for energy harvesting applications. The simulated and measured results performances are presented in Table 2.

The main purpose of this approach aims to enhance the harvesting efficiency by expanding the antenna range from one to four frequency bands in which one can harvest, rectify, and convert this unexplored ambient EM energy to a useful electric energy. However, the achieved

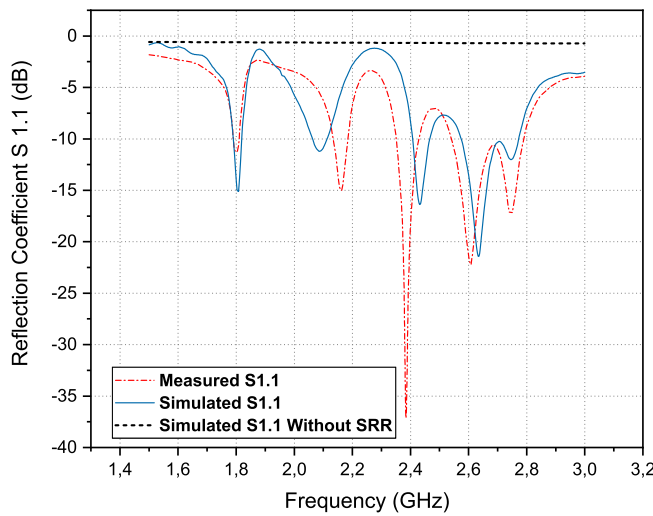


**FIGURE 3** Simulated and measured  $S_{11}$  pattern for the unit-cell CSRR multiband antenna

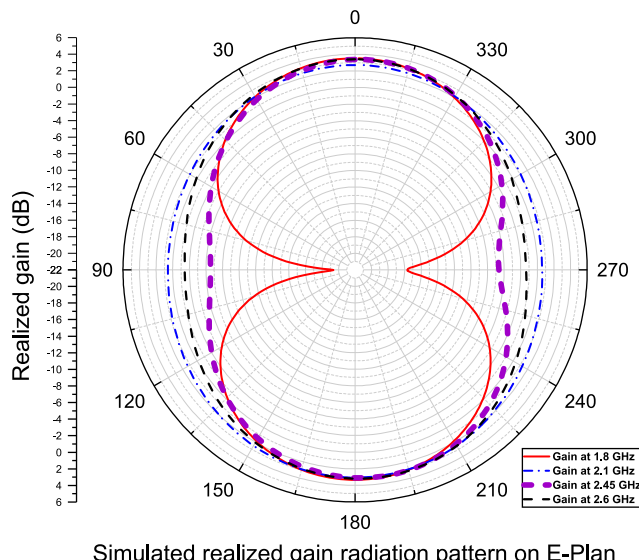
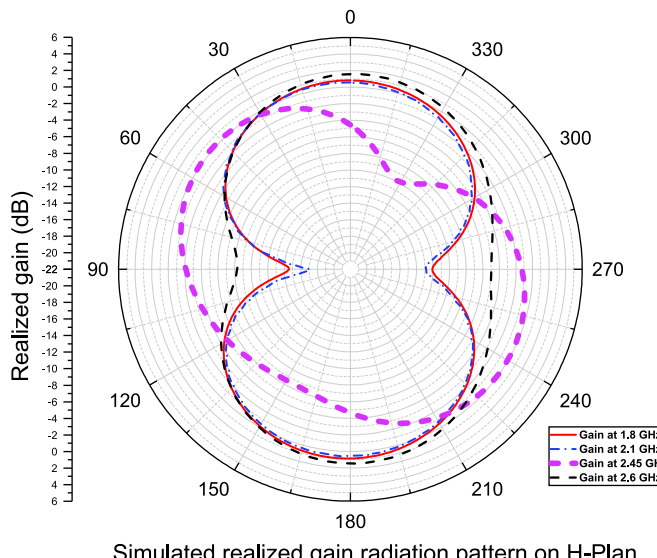


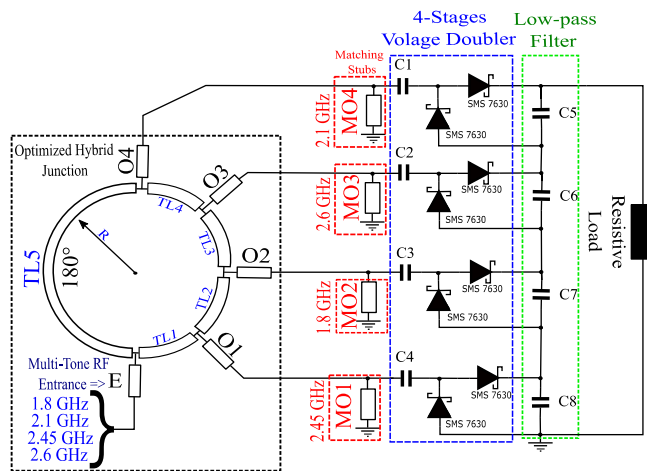
**FIGURE 4** Directive gain behavior of the final antenna at the four working frequencies



Simulated realized gain radiation pattern on H-Plan

**TABLE 2** Performances of the proposed antenna design

Resonance frequency (GHz)	Simulated $S_{11}$ (dB) without SRR	Simulated $S_{11}$ (dB)	Measured $S_{11}$ (dB)	Size reduction comparing to patch (%)	Simulated bandwidth (MHz)	Directive gain (dBi)	realized gain (dB)	Beam width (deg)
1.8	-0.61	-18.69	-11.28	63.75	32.40	3.01	2.41	85.4
2.1	-0.64	-13.03	-14.97	63.75	96.30	3.2	2.26	84
2.45	-0.67	-24.75	-10	63.75	98.22	4.25	1.58	97.7
2.6	-0.69	-13.85	-22.5	63.75	138.58	3.85	2.69	90.5

**FIGURE 5** Diagram of the quadiband optimized hybrid junction ring rectifier

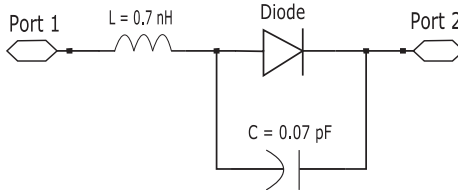
antenna can be used in numerous applications that need multiple resonance frequencies such as mobile telecommunications, sensors, or medical purposes.

### 3 | THE MODIFIED HYBRID JUNCTION MATCHING AND RECTIFYING CIRCUIT DESIGN

Rectenna's fundamental design for radio frequency energy harvesting makes it an open field for creation and innovation, where researchers have proposed various prototypes and models to diminish its size and increase its outcome. Its principle circles around the utilization of an antenna to retrieve the surrounding RF power, then, efficiently convert it into valuable DC power via an RF-DC rectifier. Naturally, in order to expand the measure of the collected RF energy, researchers tend to explore wide and multiband harvesting applications, which is by all means the most fitting methodology; however, the aforementioned applications offer an acceptable results at the expense of the size of the whole device. Since the design of the CSRR antenna has achieved a remarkable size

### SMS 7630 SPICE model parameters

$I_s = 5E-6$ A	$M = 0.4$	$F_C = 0.5$	$I_{BV,L} = 0A$
$R_s = 30 \Omega$	$E_g = 0.69$ EV	$B_v = 2$ V	$N_{BV,L} = 1$
$N = 1.05$	$X_{TI} = 2$	$I_{BV} = 1e-4$	$T_{NOM} = 27^\circ\text{C}$
$TT = 1E-11s$	$K_F = 0$	$ISR = 0$ A	$FFE = 1$
$C_{j0} = 1.4E-13F$	$A_F = 1$	$NR = 2$	
$V_j = 0.34$ V		$N_{BV} = 1$	

**FIGURE 6** SMS 7630 Spice model schema and parameters

reduction and efficiency improvement, the achieved results would be totally pointless without an innovative and effective RF-DC rectifier's design. Several attempts were made to improve the rectifier's efficiency such as in branch-line coupler use to achieve the broadband behavior,<sup>24</sup> or the use of hybrid junction, which is utilized as a power divider in order to achieve multiband function.<sup>25,26</sup> Although designing a multiband and efficient rectifier with a sufficient output voltage that has to be imprinted on a small size layouts is a significant challenge, nevertheless, in References 7, 25, 27-29 researchers have developed a very innovative designs, but unfortunately, the proposed designs exhibit some disadvantages either on the extent of the rectifier<sup>28</sup> or on the output voltage level. In Reference 28, the authors has proposed an interesting approach, where, by modifying the electrical length and characteristic impedance of each transmission line of the 180° hybrid junction ring, it can be turned to bandpass filter and divide the entering multitone signal into single-tone frequency signals, each directed to its precise output branch. Here, we extended the approach proposed in Reference 28 by adding one more band to the rectifier's design and reducing its overall size, consequently improving its efficiency and aptitude for embedded applications. Figure 5 depicts the schematic skeleton of the proposed design where  $E$  is the sum entrance of multitone signal, and O1, O2, O3, and O4

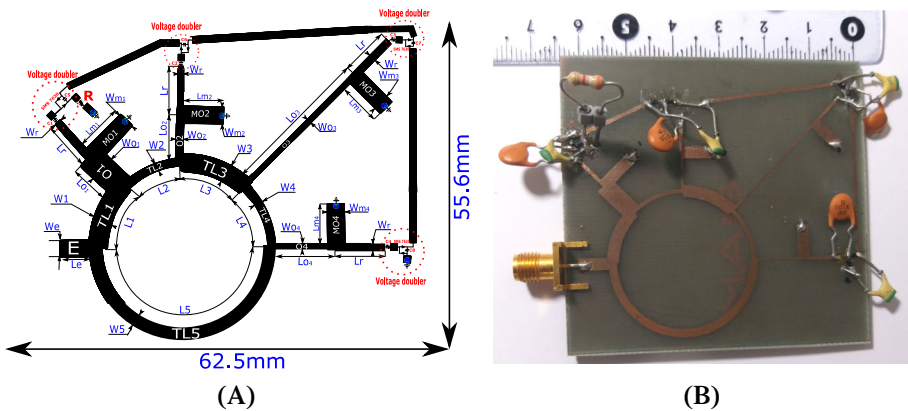


**FIGURE 7** A, Schematic and dimensions of the final layout of the optimized hybrid junction ring quadriband rectifier; B, Final multiband optimized hybrid junction ring rectifier prototype

**TABLE 3** Dimensions of the final layout for the proposed quadriband rectifier

Transmission line	Length (mm)		Width (mm)
	E	Le	
TL1	L1	10.5	W1
TL2	L2	11.5	W2
TL3	L3	10.6	W3
TL4	L4	11.25	W4
TL5	L5	43.5	W5
O1	Lo1	6.98	Wo1
O2	Lo2	6.4	Wo2
O3	Lo3	24.96	Wo3
O4	Lo4	10.2	Wo4
MO1	Lm1	8.4	Wm1
MO2	Lm2	6.8	Wm2
MO3	Lm3	7	Wm3
MO4	Lm4	7	Wm4
RECTIFIER'S T-LINE	Lr	8.1	Wr

are the modified hybrid junction ring output branches, each corresponding to a retrieved energy's frequency. The signal is filtered and divided according to the bandwidth of each output's branch, namely GSM 1.8 GHz; UMTS 2.1 GHz; WiFi 2.45 GHz and 4G 2.6 GHz. Each output branch is followed by short-circuit impedance matching stub at its own frequency band. These sections were added to endorse the filtering performance of the hybrid ring junction. In order to multiply the harvested DC power, the SMS 7630 Schottky diodes Villard voltage doubler were stacked together at the same polarity. Thus, the output voltage is eight times multiplied across the 4 kOhm resistive load. SMS 7630 Schottky diodes were chosen due to their fast transit response and low threshold voltage, which makes them suitable for high-frequency

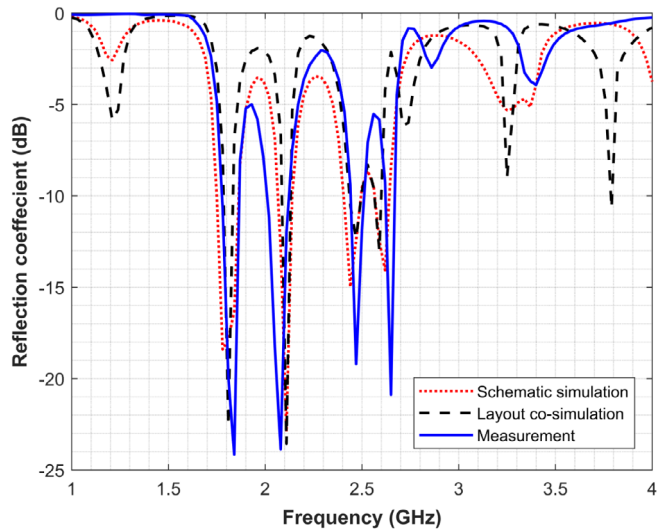


**FIGURE 8** Simulated, cosimulated, and measured reflection coefficient of the quadriband optimized hybrid junction rectifier

applications. The multiband hybrid junction ring rectifier has been designed and optimized using Keysight Advanced Design System (ADS), where a spice model for the SMS 7630 Schottky diode has been created and used to simulate its behavior.<sup>30</sup> Figure 6 depicts the schema of the spice model and its parameters. The main objective of the present work is mostly to provide an alternative solution to the conventional supplying systems, which reduces the consumed energy cost for low-consuming electronic devices and also lowers the rectifier's manufacturing cost. To this end, we sought to utilize a popular and low-cost substrate material to concept the desired design on FR4, with a relative permittivity of 4.3 and 1.58 mm of thickness.

The achieved work has been initiated by modifying and adjusting the original form of hybrid ring junction, where each transmission line's width and electrical length were tuned. Consequently, the final circuit model has achieved the filtering and signal dividing behavior as

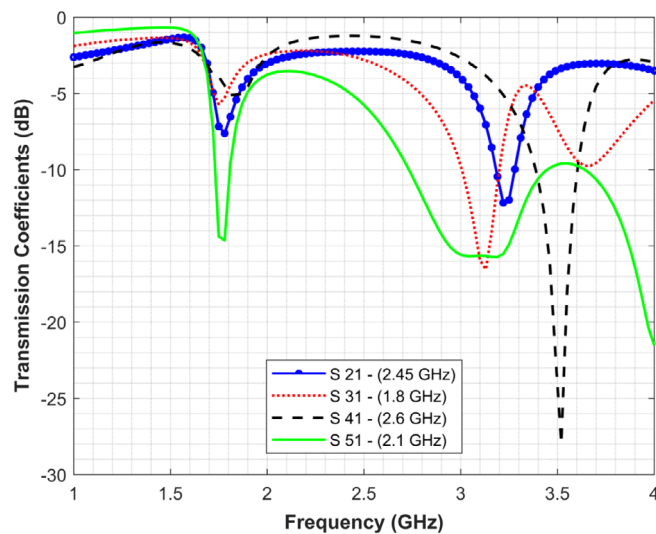


**FIGURE 9** Simulated transmission coefficients of the modified hybrid ring junction rectifier

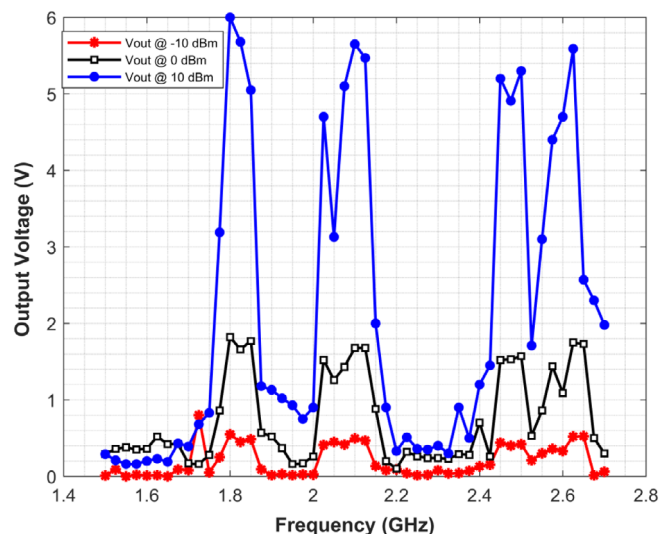


**FIGURE 11** Measured output voltage of the realized the modified hybrid junction quadri-band rectifier vs frequency

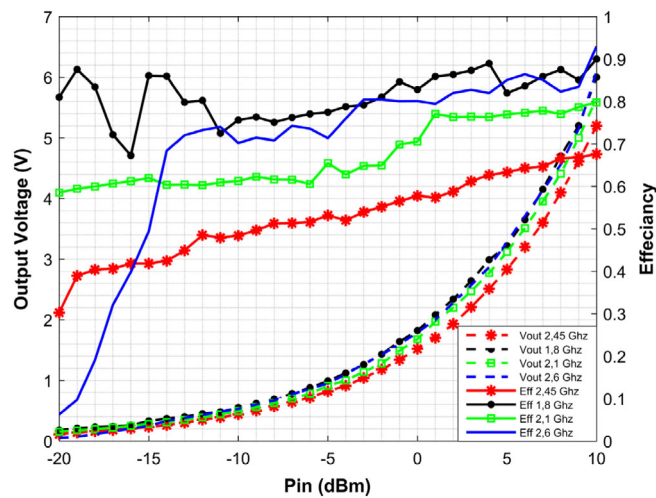


**FIGURE 10** Measured output voltage and efficiency of the realized the modified hybrid junction quadriband rectifier vs the input power

needed at the four-operation frequencies. Afterward, we matched the rectifying circuit with the output branches of modified hybrid junction ring, each to its operating frequency band. Finally, to conclude the simulation phase, a lookalike lumped component model that mimics the original schematic design behavior was generated and cosimulated to verify the validity of our approach. EM cosimulation has been proved to be an accurate tool that verifies the performance of such a schematic design.<sup>31</sup>

Figure 7A,B depicts the final design of the quadriband rectifier's layout next to realized prototype that covers a miniatuerized overall size of  $62.5 \times 55.6 \times 1.58$  mm compared

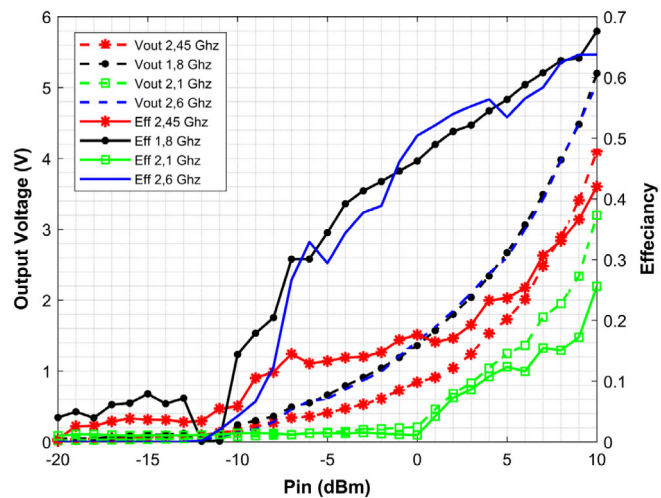


**FIGURE 12** Measured output voltage and efficiency of the realized rectenna vs the input power

with the conventional existing rectifiers. The resulted outcomes of the achieved work were realized by fixing the resistive load value to 4 kOhm, the lowpass filter capacitors C5, C6, C7, and C8 each at 10 nF and rectefier's capacitors C1, C2, C3 & C4 each at 100 pF.

The final geometrical parameters of the proposed multiband modified hybrid junction rectifier are listed in Table 3.

In Figure 8, we illustrate the simulated, cosimulated, and measured reflection coefficients of the modified hybrid junction ring rectifier. The measured reflection coefficient variations were taken by a Rohde & Schwarz ZVH4 cable and an antenna analyzer. As it is demonstrated in the figure, the reflection coefficient measurements agree well

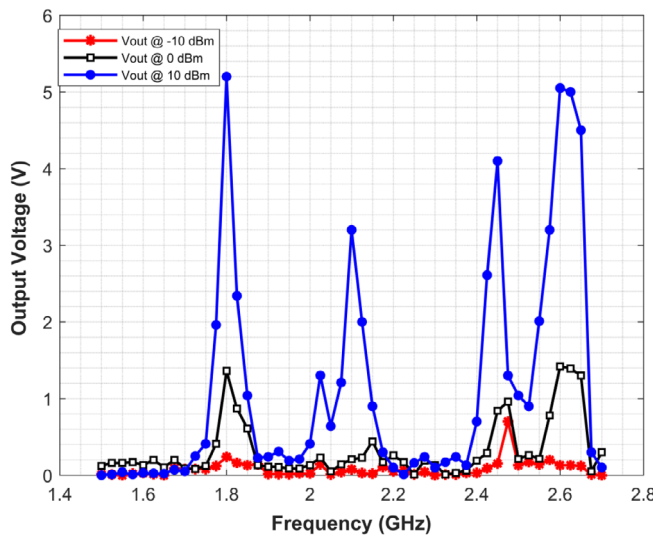


**FIGURE 13** Measured output voltage of the realized rectenna vs frequency

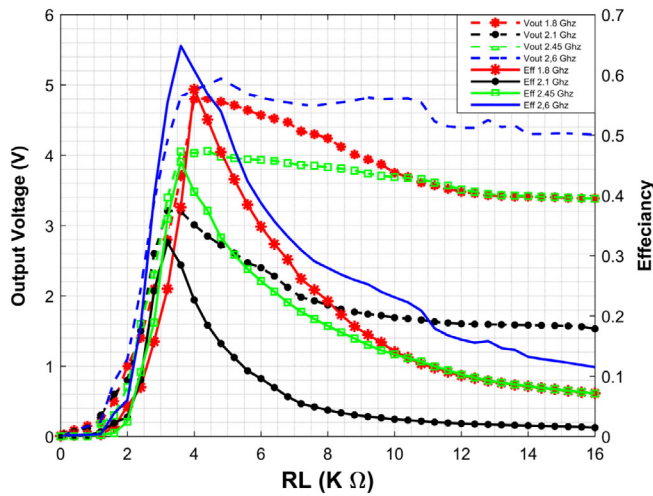


**FIGURE 14** Output voltage and efficiency analysis vs the resistive load of the rectenna

with the simulations and cosimulations where the accesses of the circuit are matched  $\leq -14$  dB at the frequency bands of interest, namely -24.2 at 1.8 GHz, -23.9 at 2.1 GHz, -19.2 at 2.45 GHz, and -21 at 2.6 GHz. We have also measured the  $-10$  dB bandwidths of the reflection coefficient at the frequency bands of interest, which are -1.782 to -1.855 GHz, 2.120 to 2.190 GHz, 2.44 to 2.51 GHz, and 2.62 to 2.67 GHz, respectively. The simulated transmission coefficients S<sub>21</sub>, S<sub>31</sub>, S<sub>41</sub>, and S<sub>51</sub> are as depicted in Figure 9 where their values are around  $-4$  dB in our frequency band of interest.

In order to evaluate the validity of our approach and the efficiency of the quadriband rectifier, and the whole rectenna prototypes, we conducted two sections of

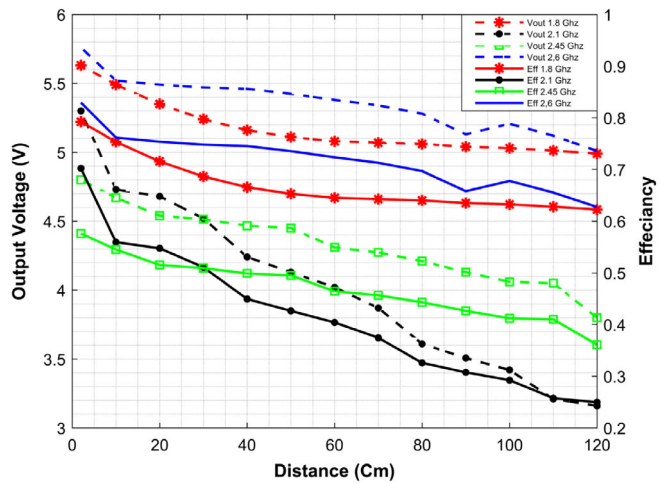


**FIGURE 15** Output voltage and efficiency analysis vs the distance of the realized rectenna



**FIGURE 16** Measurements setup in the anechoic chamber

measurement. The first starts by connecting the realized RF-DC quadriband rectifier directly to a Rohde & Schwarz SMB100A RF and a microwave signal generator and measuring the output voltage across the 4 kOhm resistive load over the frequency at three power input levels namely  $-10$ ,  $0$ , and  $10$  dBm. Then, the output voltage was measured over the input power at the frequency bands of interest. The second measurement's section has been conducted inside the anechoic chamber, where we connected the RF generator to an Hyperlog 20XXXEMI antenna and replicated the first measurements for the whole rectenna prototype being fixed at 110 cm of the Hyperlog antenna as depicted in Figure 16. These measurements in addition to the efficiency calculation have sketched a full evaluation of the performances of the rectifier and the rectenna. The efficiency can be measured as follows:

$$\eta_{RF-DC} = \frac{P_{DC}}{P_{in}} = \frac{V_{DC}^2}{P_{in} * R_L} \quad (11)$$

where  $V_{DC}$  is the DC output voltage across the load resistor,  $P_{DC}$  is the output DC power,  $P_{in}$  is the input RF power, and  $R_L$  is the load resistance.<sup>28</sup>

Figures 10 and 11 show the first section's measured output voltage and efficiency over the frequency than over the input power, respectively. One notes that the rectifier at 10 dBm input power has achieved maximum RF-DC power conversion efficiency of: 90% at 1.8 GHz, 78.9% at 2.1 GHz, 67.6% at 2.45 GHz, and 93% at 2.6 GHz, respectively. During this section, we replaced the resistive load by a Green led 703-0097 multicomp to visualize that

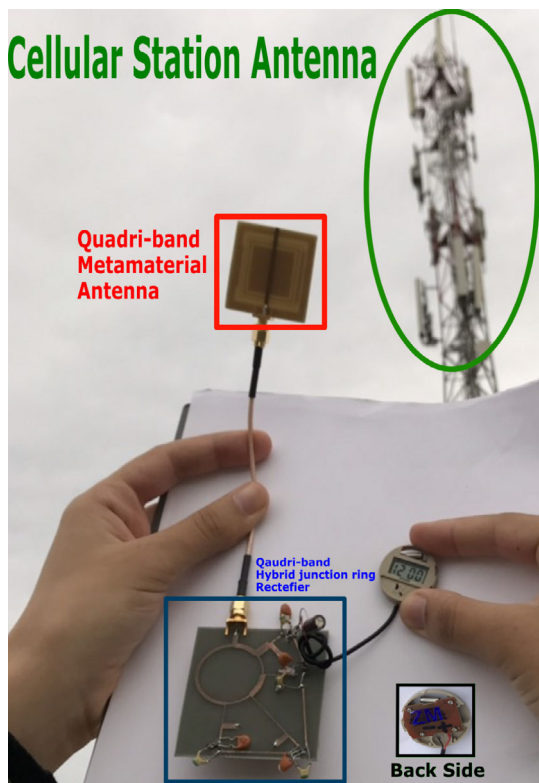


FIGURE 17 Outdoor experiment

TABLE 4 Performance comparison with recently reported rectifiers

Reference	Frequency bands (GHz)	Peak efficiency	Size (mm <sup>3</sup> )
Sun et al <sup>7</sup>	1.81-1.87, 2.11-2.17	52% at -9 dBm	145 × 55 × 0.8
Takhedmit et al <sup>25</sup>	1.8-2.45	59.2% at -5 dBm	77 × 98 × 1.5
Li Z et al <sup>28</sup>	1.74-1.97, 2-2.22, 2.41-2.59	61.7% @ 17 dBm	70 × 65 × 0.8
Çelik et al <sup>32</sup>	2.08-2.45	55% @ 3 dBm	60 × 60 × 4.6
Gozel et al <sup>26</sup>	1.7-1.925	71% @ 4.7 dBm	70 × 70 × 1.6
Wang et al <sup>3</sup>	2.45	51% @ 0 dBm	35 × 37 × 1.6
This work	1.8, 2.1, 2.45, 2.6	67.6% @ 10 dBm	62.5 × 55.6 × 1.53

the LED has switched on at 2 dBm RF input power in the frequencies 1.8, 2.1 and 2.6 GHz.

## 4 | RESULTS AND DISCUSSION

Figures 12 and 13 show the second section's measured output voltage and efficiency over the frequency then over the input power, respectively, where the whole rectenna was set at 110 cm of the Hyperlog antenna. After repeating the same measurements as in section one, we notice an important decrease in the efficiency and output voltage values, where, at 10 dBm input power, the rectenna achieved the efficiency of 67.6% at 1.8 GHz, 25.6% at 2.1 GHz, 42.025% at 2.45 GHz, and 63.75% at 2.6 GHz, respectively. Moreover, once we replace the resistive load with the led, the led switches on at 5 dBm at the frequencies of 1.8 GHz and 2.6 GHz.

More measurements have been carried out in order to provide the output voltage and efficiency analysis in function of the resistive load value and the distance that separate the HYPERLOG antenna from the rectenna prototype, where the input power has been set at  $P_{in} = 10$  dBm during this measurement. The results are presented in Figures 14 and 15, respectively.

The rectenna prototype has shown promising results during the previous measurement sections, nevertheless, these measurements were taken in a controlled environment that can never mimic the distant correspondence environment, and thus, the resulted outcome cannot be retained unless it succeeds an outdoor experiment to validate the results. To this end, we have replicated the same outdoor experiment as in<sup>28</sup> like depicted in Figure 17, where, we have connected a 220  $\mu$ F capacitor to DC output connected in parallel to a battery-less digital watch. The rectenna has efficiently converted the harvested ambient RF power to a useful DC power around cellular station antenna in a 50 m perimeter. However, the batteryless watch shows some understandable instability as we exceed that perimeter.

Table 4 illustrates the performance comparison of the realized rectenna with recently reported works at different bands. In this work, the realized rectenna converts four ambient frequency bands measuring 67.6% of peak efficiency at 10 dBm of power input at 1.8GHz compared with the covered three ambient frequencies and 61.7% of peak efficiency presented in.<sup>28</sup> Compared to the recently reported works, the presented rectenna exhibits an outstanding performance enhancement in the number of the exploited frequencies, the layout overall size and the peak efficiency.

## 5 | CONCLUSION

In this article, a novel compact energy harvesting rectenna is proposed. The realized rectenna is composed of an original and first time introduced CSRR unite cell multibands antenna and a quadriband modified hybrid junction ring rectifier. Its performances and ability to efficiently harvest the RF power at four ambient frequency bands (1.8, 2.1, 2.45, and 2.6 GHz) simultaneously have been demonstrated in both controlled and outdoor environments. The CSRR antenna exhibits a bidirectional directivity and a 63.75% size reduction compared with the conventional antenna designs. The modified hybrid junction ring rectifier has effectively converted the harvested RF power into a useful DC over the four aforementioned ambient frequency bands power up with a peak efficiency of 67.6% at 1.8 GHz. In the outdoor experiment, the suggested rectenna was able to enable a batteryless digital watch via the harvested RF power, which makes it suitable for the remote powering of low consuming devices applications.

## ORCID

Ali Benayad  <https://orcid.org/0000-0001-5947-2289>

## REFERENCES

- Sun H, Guo YX, He M, Zhong Z. Design of a high-efficiency 2.45-GHz rectenna for low-input-power energy harvesting. *IEEE Antennas Wirel Propag Lett*. 2012;11:929-932.
- Vera GA, Georgiadis A, Collado A, Via S. Design of a 2.45 GHz rectenna for electromagnetic (EM) energy scavenging. *2010 IEEE Radio Wirel Symp RWW*. 2010;61-64.
- Wang M, Yang L, Fan Y, Shen M, Li Y, Shi Y. A compact omnidirectional dual-circinal rectenna for 2.45 GHz wireless power transfer. *Int J RF Microw Comput Eng*. 2019;29(1):1-7.
- Desa H, Sofian M, Zairi S. Study of integration 2.4GHz and 5.8GHz in RFID tag. *Proc Int Conf Man-Machine Syst*. 2009; 11-13.
- Harouni Z, Cirio L, Osman L, Gharsallah A, Picon O. A dual circularly polarized 2.45-GHz rectenna for wireless power transmission. *IEEE Antennas Wirel Propag Lett*. 2011;10:306-309.
- Ho DK, Kharrat I, Ngo VD, Vuong TP, Nguyen QC, Le MT. Dual-band rectenna for ambient RF energy harvesting at GSM 900 MHz and 1800 MHz. *IEEE Int Conf Sustain Energy Technol ICSET*. 2017;1:306-310.
- Sun H, Guo YX, He M, Zhong Z. A dual-band rectenna using broadband yagi antenna array for ambient rf power harvesting. *IEEE Antennas Wirel Propag Lett*. 2013;12:918-921.
- Khemar A, Kacha A, Takhedmit H, Abib G. Design and experiments of a dual-band rectenna for ambient RF energy harvesting in urban environments. *IET Microwaves, Antennas Propag*. 2017;12(1):49-55.
- Bakır M, Karaaslan M, Altıntaş O, Bagmanlı M, Akdogan V, Temurtaş F. Tunable energy harvesting on UHF bands especially for GSM frequencies. *Int J Microw Wirel Technol*. 2018;10(1):67-76.
- Arrawatia M, Baghini MS, Kumar G. Broadband rectenna array for RF energy harvesting. *IEEE Antennas Propag Soc Int Symp APSURSI 2016 - Proc*. 2016;2016:1869-1870.
- Ye H, Chu Q. A broadband rectenna for harvesting low-power RF energy. *2016 International Symposium on Antennas and Propagation (ISAP)*; 2016:46-47.
- Veselago VG. The electrodynamics of substances with simultaneously negative values of  $\epsilon$  and  $\mu$ . *Sov Phys Uspekhi*. 1968;10:509-514.
- Shalin AS, Ginzburg P, Orlov AA, et al. Optical cloaking with ENZ-metamaterials. *9th Int Congr Adv Electromagn Mater Microwaves Opt Metamaterials 2015* 2015:487-489.
- Marqués R, Ferran Martín MS. *Metamaterials with Negative Parameters: Theory, Design, and Microwave Applications*. New York: Wiley Interscience; 2008.
- Wu MF, Meng FY, Wu Q, Wu J, Li LW. A compact equivalent circuit model for the SRR structure in metamaterials. *Asia-Pacific Microw Conf Proc*. 2005;1:5-8.
- Wu Q, Wu M-F, Meng F-Y, Wu J, Li J. Research on SRR structure metamaterial based on transmission line theory. *Dianbo Kexue Xuebao/Chinese J Radio Sci*. 2006;21:310-314.
- Wu Q, Wu MF, Meng FY, Wu J, Li LW. Modeling the effects of an individual SRR by equivalent circuit method. In: *IEEE Antennas and Propagation Society, AP-S International Symposium (Digest)*. 2005.
- Salim A, Lim S. Complementary split-ring resonator-loaded microfluidic ethanol chemical sensor. *Sensors (Switzerland)*. 2016;16(11).
- Albishi A, Ramahi OM. Detection of surface and subsurface cracks in metallic and non-metallic materials using a complementary split-ring resonator. *Sensors (Switzerland)*. 2014; 14(10):19354-19370.
- Baena JD, Bonache J, Martín F, et al. Equivalent-circuit models for split-ring resonators and complementary split-ring resonators coupled to planar transmission lines. *IEEE Trans Microw Theory Tech*. 2005;53(4 II):1451-1460.
- Falcone F, Lopetegi T, Laso MAG, et al. Babinet principle applied to the design of metasurfaces and metamaterials. *Phys Rev Lett*. 2004;93(19).
- Marqués R, Baena JD, Martín F, Bonache J. FJ left-handed metamaterial based on dual split ring resonators in microstrip. *Proc Int URSI*. 2004;1:23-27.
- Mohan S. The Design, Modeling and Optimization of On-Chip Inductor and Transformer Circuits. Stanford University, Dissertation Thesis. 1999.
- Zhang XY, Du ZX, Xue Q. High-efficiency broadband rectifier with wide ranges of input power and output load based on

- branch-line coupler. *IEEE Trans Circuits Syst I Regul Pap.* 2017;64(3):731-739.
25. H. Takhedmiti, L. Cirio, Z. Saddii J.D. Lan Sun Luk A novel dual-frequency rectifier based on a 1800 hybrid junction for RF energy harvesting. 7th Eur Conf Antennas Propag (EUCAP 2013)—Conv Sess A. 2013;1,2472–2475.
  26. Gozel MA, Kahriman M, Kasar O. Design of an efficiency-enhanced Greinacher rectifier operating in the GSM 1800 band by using rat-race coupler for RF energy harvesting applications. *Int J RF Microw Comput Eng.* 2019;29(1):1-8.
  27. Jeong J, Jeong Y. A novel dual-band RF energy harvesting circuit with power management unit for low power applications. *Microw Opt Technol Lett.* 2017;59(8):1808-1812.
  28. Li Z, Zeng M, Tan HZ. A multi-band rectifier with modified hybrid junction for RF energy harvesting. *Microw Opt Technol Lett.* 2018;60(4):817-821.
  29. Ozturk B, Coskun O. Design of wideband microstrip power divider/combiner with input and output impedance matching for RF energy harvesting applications. *Int J RF Microw Comput Eng.* 2019;29(1):1-7.
  30. Alpha Industries Level Detector Design for Dual-Band GSM-PCS Handsets Square Law and Linear Response. APN1014.
  31. Syuhaimi K, AbdulMalek MEM. Circuit co-simulation: a highly accurate method for microwave amplifier design. *Univers J Comput Sci Eng Technol.* 2010.
  32. Çelik K, Kurt E. A novel meander line integrated E-shaped rectenna for energy harvesting applications. *Int J RF Microw Comput Eng.* 2019;29(1):1-10.

## AUTHOR BIOGRAPHIES



**Ali Benayad** was born in Algeria in 1990. He received his Master degree in the field of Instrumentation Engineering from the Faculty of Electronic and Computer Sciences, USTHB University, Algiers, Algeria, in 2013. Actually, he is working toward the PhD degree

in the same faculty. His research interests include microwave circuits, RF energy harvesting, antennas, and biomedical devices.



**Mohamed Tellache** was born in Algeria in 1960. He received the Engineering degree in Electrical Engineering from the Ecole Nationale Polytechnique of Algiers in 1985. He received his Master degree in 1988 in Electronic Communication from Ottawa University, Canada, and the PhD degree in 2008 in Telecommunications from USTHB, Algeria. During 1995/1998, he spent 18 months at the Electronics Laboratory of INP-ENSEEIHT, Toulouse, France, working principally on microwaves technology and modeling. He was the Head of the High School of Technology during 2009 to 2012, and before this, the Head of the Telecommunications Department in USTHB. Presently, he is a Professor of Electrical Engineering at the faculty of Electronics and Computers of USTHB, working on the development of new algorithms for modeling microwave devices, numerical methods for electromagnetism, full wave characterization of microwave circuits, microwave and components design, and communication systems.

**How to cite this article:** Benayad A, Tellache M. A compact energy harvesting multiband rectenna based on metamaterial complementary split ring resonator antenna and modified hybrid junction ring rectifier. *Int J RF Microw Comput Aided Eng.* 2020;30: e22031. <https://doi.org/10.1002/mmce.22031>